

# Three-Dimensional Assessment of Myocardial Oxidative Metabolism: A New Approach for Regional Determination of PET-Derived Carbon-11-Acetate Kinetics

Jörg Kotzerke\*, Rodney J. Hicks, Edwin Wolfe, William H. Herman, Edgar Molina, David E. Kuhl, and Markus Schwaiger

*Division of Nuclear Medicine, Department of Internal Medicine, The University of Michigan Hospitals, Ann Arbor, Michigan*

We have developed a new analysis algorithm which generates polar coordinate maps of myocardial carbon-11-<sup>(11)C</sup> acetate kinetics. In 10 normal subjects ( $n = 20$  studies), myocardial <sup>11</sup>C clearance rate constants ( $k$ ) averaged  $0.057 \pm 0.009$  (per minute). Regional  $k$ -values varied only  $10.6 \pm 2.4\%$  in the normal left ventricle. However, there was a small but significant segmental variation with increased <sup>11</sup>C clearance in the septal, anterior, and basal regions ( $p < 0.05$ ). Since <sup>11</sup>C clearance rates reflect tri-carboxylic acid cycle flux, these results suggest that myocardial oxidative metabolism is relatively homogeneous in the normal human heart at rest with minor regional variations, which possibly reflect varying regional wall stresses or substrate utilization. The proposed approach provides three-dimensional evaluation of regional oxidative metabolism which will permit characterization of the location, extent, and severity of myocardial disease.

*J Nucl Med* 1990; 31:1876–1893

The ability to noninvasively characterize myocardial oxidative metabolism may significantly improve the evaluation of the metabolic concomitants of diverse cardiac diseases and the response of these to therapeutic interventions. Carbon-11-<sup>(11)C</sup> acetate has been introduced as a tracer for the assessment of oxidative metabolism using positron emission tomography (PET). Carbon-11-acetate is avidly taken up by the myocardium and metabolized through the tri-carboxylic acid (TCA) cycle with release of <sup>11</sup>C CO<sub>2</sub>. Myocardial <sup>11</sup>C clearance kinetics are, thus, a marker of TCA cycle flux and have been shown to reliably reflect myocardial oxygen con-

sumption in animal and clinical studies (1,2). Carbon-11-acetate is a preferred substrate for the TCA cycle and, unlike alternative metabolic tracers such as <sup>11</sup>C-palmitate and fluorine-18-fluorodeoxyglucose, its oxidation appears to be largely independent of plasma substrate availability (3). Previous clinical investigations have determined <sup>11</sup>C-acetate uptake and clearance kinetics using region of interest analysis of a limited number of transverse image sets (4,5). The inferior wall of the left ventricle is poorly defined on the transverse image set and, hence, only limited evaluation of the spatial distribution of <sup>11</sup>C-acetate kinetics is possible by this approach. New instrumentation, allowing simultaneous image acquisition of multiple, contiguous cross-sectional images encompassing the entire heart and software which permits reorientation of the acquired image sets in relation to the cardiac long-axis, has provided the opportunity to assess the three-dimensional distribution of cardiac perfusion, metabolism, and function. In order to fully utilize the benefits of state-of-the-art instrumentation and computer support, we have developed a rapid, semi-automated regional analysis and curve-fitting algorithm which generates quantitative polar coordinate maps of myocardial <sup>11</sup>C uptake and clearance.

The specific aims of this study were as follows: First, to validate this new analysis algorithm by comparison with a conventional approach, which is similar to that used by other investigators. Second, to assess the three-dimensional homogeneity of oxidative metabolism in the normal human heart, as reflected by regional <sup>11</sup>C-acetate clearance kinetics. Third, to assess the influence of varying substrate availability on global and regional myocardial <sup>11</sup>C kinetics.

## METHODS

### Study Population

Ten healthy male volunteers, aged 22 to 29 yr (mean 25.7  $\pm$  2.8 yr), were enrolled as controls for comparison with

Received Jan. 8, 1990; revision accepted April 18, 1990.

For reprints contact: Markus Schwaiger MD, Division of Nuclear Medicine, Department of Internal Medicine, University of Michigan Hospitals, B1 G412, Ann Arbor, MI 48109-0028.

\* Current address: Abteilung Nuklearmedizin und spez. Biophysik Medizinische Hochschule, Hannover, West Germany.

patients studied in various ongoing PET research protocols investigating cardiac disease. None of the normal volunteers had known metabolic or cardiac disease based on clinical history and physical examination, nor known drug use. All had normal resting electrocardiographs and subjects undergoing euglycemic insulin clamp studies had previously had a normal oral glucose tolerance test.

### Study Protocols

All subjects ( $n = 10$ ) were fasted overnight. The population was divided into two study protocols. The first five subjects underwent dynamic PET imaging with  $^{11}\text{C}$ -acetate initially fasting and subsequently 30–60 min after a 50-gram oral glucose load. This protocol was performed in order to assess the effect of oral glucose loading on global and regional  $^{11}\text{C}$ -acetate uptake and clearance.

The other five subjects underwent two studies, performed one to seven days apart to assess the effect of increased free-fatty acid (FFA) availability on  $^{11}\text{C}$ -acetate uptake and clearance. Both studies involved a euglycemic clamp as described by DeFronzo et al. (6). One study was performed with and the other without infusion of FFAs (Intralipid 20% at 1 ml/min). Dynamic PET  $^{11}\text{C}$ -acetate imaging was performed under steady-state glucose conditions, which were achieved ~45 min after beginning the clamp procedure. At the beginning of the  $^{11}\text{C}$ -acetate study in subjects from this group, venous blood was collected for measurement of glucose and FFAs. These values were obtained after at least 45 min of glucose, insulin, and, in the second studies, FFA infusion. All subjects had heart rate, blood pressure, and ECG monitoring throughout the investigations.

### Positron Emission Tomography Acquisition Protocol

Carbon-11-acetate was synthesized utilizing the technique described by Pike et al. (7). PET was performed using a whole-body PET scanner (Siemens 931, Hoffman Estates, IL), which has eight circular detector rings to allow for the simultaneous acquisition of 15 contiguous transaxial images with a slice thickness of 6.75 mm. The reconstructed image resolution of this system is 6 mm at full width at half maximum (FWHM) in-plane and 8 mm FWHM axially using line source phantoms. Transmission data were acquired prior to the emission studies in order to correct for the effect of photon attenuation on the emission images. Following intravenous administration of 740 MBq (20 mCi)  $^{11}\text{C}$ -acetate over 30 sec, dynamic PET imaging was performed over 31 min in frame mode, 128  $\times$  128 matrix acquisition. Ten frames (defined as an image set of all 15 planes) were acquired for 90 sec, and were followed by five frames of 120 sec duration, and finally, two frames of 180 sec duration. With this imaging protocol, there were typically six to eight million counts in the initial frame, reflecting the significant blood-pool activity at this time, and between two and three million counts in the final frame. Typically, planes incorporating the mid-ventricular region had ~600,000 counts in the early frames and 200,000 counts in the late frames.

### Three-Dimensional Reorientation Algorithm

The PET system routinely provides reconstructed transverse images orientated perpendicular to the sagittal and coronal planes of the body. Therefore, we performed image

processing in order to create 12 transaxial images reoriented in the short-axis of the heart (Fig. 1) using a dedicated workstation (Sun Microsystems Inc.). The vertical and horizontal cardiac long-axis angles were defined using the frame with the highest myocardial activity (3–6 min after tracer injection) and were subsequently used for the reorientation of all 17 frames. The algorithm used is similar to that previously proposed for reorientation of thallium-201 single-photon emission computed tomography (SPECT) images (8) and rubidium-82 PET studies (9).

### Regional Data Analysis

The reoriented, short-axis images served as input data to a semi-automated regional analysis program newly developed at our institution, which creates polar coordinate maps of  $^{11}\text{C}$  myocardial uptake and clearance. This program involved assignment of ellipses which enclose the myocardial activity in each of the approximately 12 short-axis images of the frame with the best myocardial definition. The operator identified the posterior intersection of the right and the left ventricles on one of the short-axis images. A radius was automatically interpolated between the center of the defined ellipse and this point (8). This radius represents the starting point of 60 equidistant radii which were used to define circumferential profiles of regional activity distribution in each plane. The program performed a search for the maximum average activity in a  $3 \times 3$  pixel area along each radius and within the ellipse,

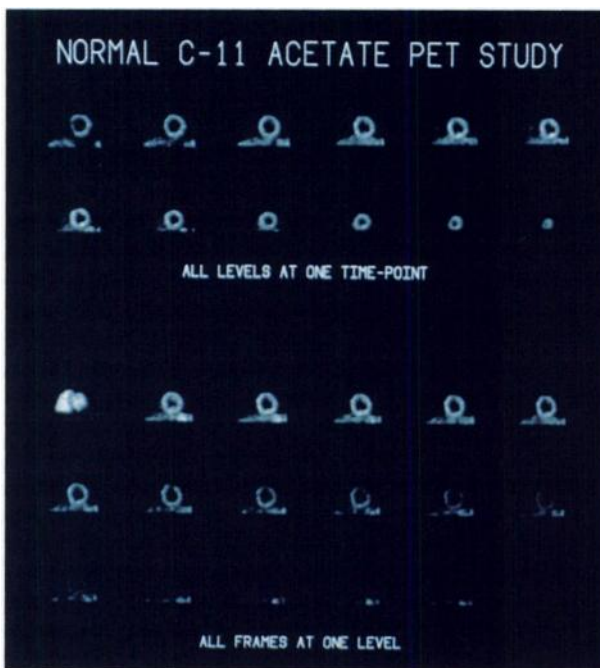


**FIGURE 1**

A representative example of 12 short-axis cardiac planes (upper panel) obtained 9 min following  $^{11}\text{C}$ -acetate administration in a normal subject demonstrates excellent myocardial definition. The planes are arranged from base to apex. In the same subject, all 17 acquisition frames (lower panel) are displayed for a single mid-ventricular plane. The initial image shows activity in the left and right ventricular cavities. There is rapid clearance of blood-pool activity and uptake by the myocardium. Subsequently, significant clearance of  $^{11}\text{C}$  activity with time is apparent.

defining a myocardial region of interest (ROI) for each short-axis image. These circumferential ROIs in each short-axis image were then propagated to all frames thereby defining a time-activity curve for that 3 pixel  $\times$  3 pixel (7 mm  $\times$  7 mm)  $\times$  8 mm voxel. In addition, a small blood-pool ROI is drawn on one to three basal planes. The most basal planes were selected because they have the largest ventricular diameter minimizing the spill-over from myocardial activity at late time points. Based on data reported by Walsh (10), monoexponential, least-squares curve fitting was applied to the 60 time-activity curves generated by the regional analysis algorithm for each short-axis plane (Fig. 2). The time point used to begin fitting the myocardial  $^{11}\text{C}$  clearance curves was selected by visual inspection of myocardial and blood-pool time-activity curves of summed data in a single mid-ventricular plane.

Each ROI time-activity curve was defined by a myocardial clearance and an amplitude. The amplitude was derived from extrapolation of the clearance time-activity curve to time zero of curve fitting and provides an index of instantaneous myocardial  $^{11}\text{C}$  uptake which has been shown to reflect myocardial blood flow (1). The amplitude of each of the 60 time-activity curves in each plane was divided by the maximum amplitude obtained within the heart to obtain a relative amplitude which provided an index of relative  $^{11}\text{C}$ -acetate uptake expressed as percent. The relative amplitude and  $^{11}\text{C}$  clearance rate constant data for each sector of all 12 short-axis images were displayed as a polar coordinate map.

The polar map display was subsequently divided into sec-

tors to provide regional data analysis. Mean values and standard deviations of the relative amplitude of  $^{11}\text{C}$ -acetate uptake and the  $^{11}\text{C}$  clearance constant data were given for four sectors (anterior, lateral, inferior and septal). Nine segments were defined by summing data from five basal planes, and from five mid-ventricular planes for each of four sectors and from the entire two apical planes (Fig. 3). In order to compare the data derived using this new regional analysis algorithm with data relating to  $^{11}\text{C}$  clearance kinetics published by others (1, 4–5, 10) from analysis of transverse, nonreoriented mid-ventricular images, a second ROI analysis was performed on a transverse, mid-ventricular image from each study. Septal, anterior, anterolateral, and lateral wall myocardial ROIs and a small left ventricular blood pool ROI were manually defined on a mid-ventricular plane and extrapolated to each frame to generate tissue  $^{11}\text{C}$  time-activity curves for each ROI. Least-squares, monoexponential curve fitting was applied following visual determination of the commencement of each myocardial clearance curve.

### Statistical Analysis

Values are given as mean  $\pm$  s.d. Regional values of amplitude and  $^{11}\text{C}$  clearance rate constants were compared using Student's t-test for paired data with Bonferroni's correction for multiple analyses. Similarly, comparison of the effects of changing substrate availability on global and regional  $^{11}\text{C}$ -acetate kinetics, hemodynamic and biochemical data were assessed by comparison of the results obtained in the two studies performed in any given individual using Student's t-test for paired data. Statistical significance was defined as p values  $\leq 0.05$ .

## RESULTS

### Hemodynamic and Biochemical Findings

Heart rate in the 20 studies averaged  $58 \pm 7$  bpm. The mean arterial blood pressure averaged  $112 \pm 8$  mm Hg, and the rate-pressure product ranged from 5160 to 8614 with an average of 6420 (mm Hg  $\times$  bpm). The glucose level averaged  $94 \pm 24$  mg/dl. The average glucose level in the fasting subjects was 89 mg/dl and rose to 120 mg/dl following oral glucose load. There was no significant difference between the glucose levels in the clamp studies. In the insulin clamped subjects, FFA levels obtained immediately prior to the  $^{11}\text{C}$ -acetate study, i.e., after 45 min of glucose and insulin infusion, averaged 100 mmol/l in the initial studies and 400 mmol/l following FFA infusion (Table 1).

### Myocardial Uptake of $^{11}\text{C}$ -acetate

A representative example of 12 resliced short-axis images for an early frame with the high myocardial  $^{11}\text{C}$  activity in a normal subject at rest is illustrated in the upper panel of Figure 1. The lower panel demonstrates all 17 frames of a mid-ventricular short-axis plane. Initial activity corresponding to blood pool is followed by rapid myocardial uptake and blood-pool clearance. Subsequent clearance of myocardial activity with time is clearly apparent on the series of 17 frames. The relative amplitude, a marker of  $^{11}\text{C}$ -acetate uptake, av-

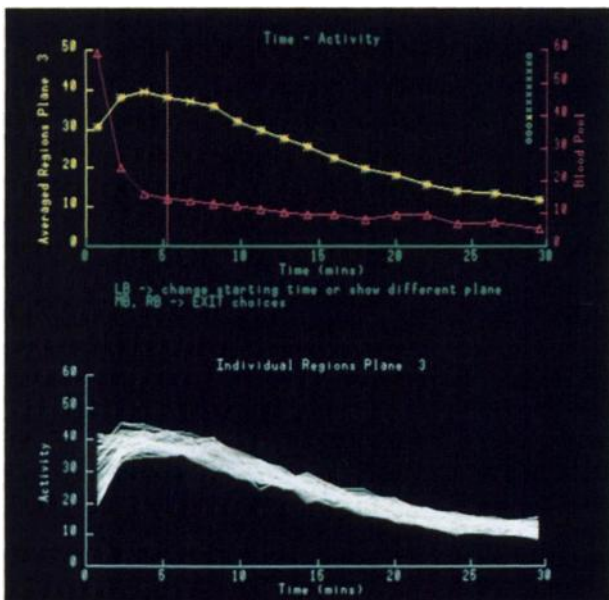


**FIGURE 2**

A time-activity curve (upper panel) representing the summed data of 60 sectors in a single plane are demonstrated for both, myocardial (yellow) and blood-pool (red) ROIs. The commencement time (orange) for fitting of a monoexponential myocardial clearance curve is determined by visual analysis of these two curves. In particular, the end of the transient high activity blood-pool phase is noted. The individual time-activity curves for each of the 60 sectors (lower panel) in this plane demonstrate the overall homogeneity of uptake and clearance kinetics.

TABLE 1

Comparison of Hemodynamic and Metabolic Parameters with  $^{11}\text{C}$ -acetate Washout Under Different Dietary Conditions

Dietary state	n	Average $k^*$ (per min)	syst. BP (mm Hg)	HR (bpm)	DP <sup>†</sup>	Glucose (mg/dl)	FFA <sup>§</sup> (mmol/l)
Fasted	5	0.058 ± 0.015	107 ± 5	59 ± 3	6317 ± 362	89 ± 9	n.d.
Oral glucose	5	0.055 ± 0.007	112 ± 9	62 ± 7	6924 ± 1202	120 ± 42	n.d.
Eu clamp <sup>¶</sup>	5	0.053 ± 0.006	117 ± 5	54 ± 8	6319 ± 866	88 ± 10	100 ± 10
Eu clamp + FFA	5	0.061 ± 0.006	111 ± 10	55 ± 7	6120 ± 679	85 ± 13	400 ± 100
All studies	20	0.057 ± 0.009	112 ± 8	58 ± 7	6420 ± 826	94 ± 24	

<sup>\*</sup>  $k = {^{11}\text{C}}$  washout rate constant.<sup>†</sup> DP = Rate pressure product (beats per min × systolic BP).<sup>§</sup> FFA = Free-fatty acids.<sup>¶</sup> Eu Clamp = Euglycemic insulin clamp.

n.d. = not done.

eraged  $74.4\% \pm 12.0\%$  for the reoriented short-axis images in individual studies (Table 2). Regional variations in myocardial uptake were minor (Table 3). There was no significant difference between myocardial uptake in the anterior, septal, lateral, and inferior walls. However,  $^{11}\text{C}$ -acetate uptake in the apex was significantly lower than that in the mid-ventricular and basal regions ( $p < 0.05$ ). No significant difference was found between uptake in the mid-ventricular and in the basal regions.

#### Myocardial Clearance of $^{11}\text{C}$ -Acetate

**Comparison of Regional Analysis Algorithms.** The average myocardial clearance rate constant values derived from reoriented short-axis and transverse images agreed closely and were strongly correlated ( $y = 1.03x - 0.0001$ ,  $r = 0.92$ ) (Fig. 4). Regional analysis of clearance rate constant values in individual studies by both ROI analysis techniques showed relatively homogeneous activity throughout the heart with variations of 10.6% and 14%, respectively (Fig. 3).

**Clearance Rate Constant Data for Short-Axis Images.** Comparison of paired regional  $^{11}\text{C}$  clearance rate constants in individual studies demonstrated significant, albeit small, regional variation. The anterior and septal sectors had higher  $^{11}\text{C}$  clearance rates (by ~5%) than the lateral sector ( $p < 0.05$ ). The  $^{11}\text{C}$  clear-

ance was lower in the inferior wall than in the septum and anterior wall but failed to reach statistical significance after Bonferroni correction (Fig. 4). Carbon-11 clearance rate constants were higher (by ~4%) in the basal segments of the heart compared with the mid-ventricular segments which were, in turn, higher (by ~8%) than in the apical segment. This gradient was significant ( $p < 0.05$ ) (Table 4 and Fig. 5).

**Effect of Substrate Availability on  $^{11}\text{C}$  Clearance Kinetics.** Paired analysis of  $^{11}\text{C}$  clearance rate constants averaged for the entire heart in the fasting and oral glucose-loaded studies demonstrated no significant change, although  $^{11}\text{C}$  clearance was 5% higher in the fasting state. In the insulin-clamped subjects, global  $^{11}\text{C}$  clearance increased significantly with the addition of FFA infusion ( $p < 0.05$ ) (Fig. 6). This was reflected in the average  $^{11}\text{C}$  clearance constant of the studies with FFA infusion being 15% higher than in those without. The increase was most marked in the septal wall (Tables 2 and 4).

Myocardial oxygen consumption is determined by loading conditions of the ventricle. Since there was a lower average left ventricular double product in the fasting group of studies, it appears unlikely that the higher observed global  $^{11}\text{C}$  clearance for these studies is due to increased left ventricular loading. Similarly, the higher average  $^{11}\text{C}$  clearance in the studies with FFA

TABLE 2  
Global  $^{11}\text{C}$ -acetate Uptake and Washout ( $k$ -value) Under Different Dietary Conditions

Dietary state	n	Uptake	s.d. <sub>o</sub> (%) <sup>*</sup>	Range	k-value <sup>†</sup>	s.e. <sub>o</sub> (%) <sup>*</sup>	Range
Fasted	5	76.1	11.2	67.8–82.3	0.058	9.8	0.044–0.081
Oral glucose	5	73.5	11.4	68.7–76.6	0.055	9.2	0.047–0.064
Eu clamp	5	75.5	12.8	71.7–81.8	0.053	12.2	0.049–0.064
Eu clamp + FFA	5	72.5	12.6	70.1–77.5	0.061	11.1	0.052–0.069
All studies	20	74.5	12.0	67.8–81.8	0.057	10.6	0.044–0.081
s.d.		4.0	2.0		0.009	2.4	

<sup>\*</sup> Intrastudy standard deviation which is an indicator of homogeneity within individual studies.<sup>†</sup>  $p < 0.05$  for i.v. clamp versus i.v. clamp + FFA.

**TABLE 3**  
Regional  $^{11}\text{C}$ -acetate Uptake Under Different Dietary Conditions

Dietary state	Septal	Anterior	Lateral	Inferior	Apex	Mid-ventricular	Basal
Fasted <sup>†</sup>	78.6	75.3	75.0	75.6	66.9	77.3	78.4
Oral glucose <sup>‡</sup>	74.1	71.0	74.7	74.1	64.7	74.7	75.3
Eu clamp <sup>§</sup>	75.1	74.5	75.4	75.7	65.4	76.9	75.7
Eu clamp + FFA <sup>¶</sup>	73.7	73.3	72.1	72.4	64.6	74.7	73.9
All studies <sup>**</sup>	75.4	73.5	74.3	74.4	64.4	75.9	75.8
s.d.	4.5	4.9	5.0	4.5	5.5	4.7	4.6

<sup>†</sup> p < 0.05 for apex versus mid-ventricular and basal and anterior versus septal.

<sup>‡</sup> p < 0.05 for apex versus mid-ventricular.

<sup>§</sup> p < 0.05 for apex versus mid-ventricular.

<sup>¶</sup> p < 0.05 for apex versus mid-ventricular and basal.

<sup>\*\*</sup> p < 0.05 for apex versus mid-ventricular and basal.

infusion was present despite a lower average left ventricular double product in this group of studies (Table 1). When normalized for left ventricular double product, global  $^{11}\text{C}$  clearance rate constants were 16% higher under fasting conditions than those following oral glucose load, and 19% higher in the FFA-loaded clamp studies than in those without FFA infusion ( $p < 0.05$ ).

## DISCUSSION

Using state-of-the-art PET instrumentation and advanced image processing, polar maps of regional physiologic processes such as blood flow, metabolism, and function can be obtained. A parametric display approach has been employed for  $^{11}\text{C}$ -acetate kinetics to assess the regional  $^{11}\text{C}$ -acetate uptake and clearance kinetics as markers of perfusion and oxidative metabolism in the human heart.

### Technical Considerations

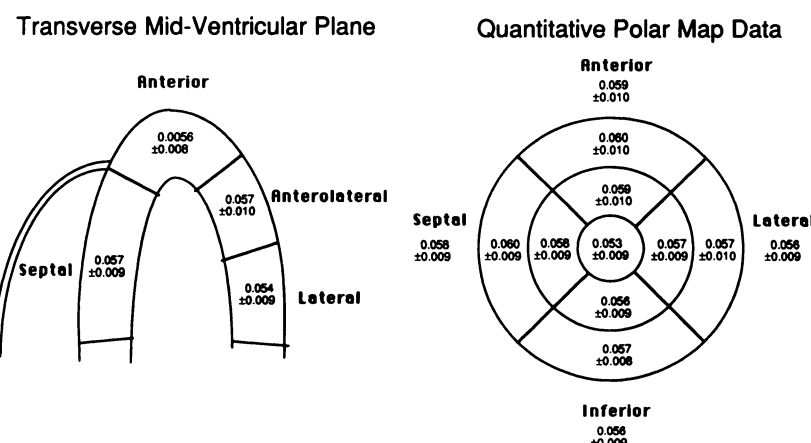
The newly developed processing software includes three-dimensional reorientation of cardiac images, multi-plane ROI assignment, automated curve fitting routines, and standardized data display. The results of this integrated approach to the analysis of myocardial  $^{11}\text{C}$ -acetate kinetics agreed closely with those obtained from conventional analysis of transverse PET images.

However, the proposed data processing approach offers several major advantages. First, it allows improved analysis of the inferior and posterior walls of the heart which are difficult to assess on the transverse planes. Second, it provides a standardized, parametric representation of  $^{11}\text{C}$  kinetics in three-dimensions with objective quantification of regional variation in a widely accepted format (8,9,14). Third, the generation of polar coordinate maps of  $^{11}\text{C}$  clearance allows comparison of individual polar coordinate maps with a normal database independent of individual variation in anatomical orientation of the heart.

Determination of myocardial oxidative metabolism from  $^{11}\text{C}$ -acetate clearance kinetics poses multiple potential methodologic problems. Ideally, analysis of  $^{11}\text{C}$  clearance from the myocardium should correct for the effects of spillover of blood-pool activity. However, data published by Armbrecht et al. (4) suggests that uncorrected and spill-over corrected rate constants correlate closely. Under conditions of increased physiologic stress,  $^{11}\text{C}$  clearance kinetics are biexponential with a rapid and a slow exponent. Monoexponential curve fitting under these situations yields a significant underestimation of true oxidative metabolism (11). However, under normal resting physiologic conditions in the hu-

### FIGURE 3

Mean regional  $^{11}\text{C}$  clearance constants ( $k$ ) for the entire study population, as assessed by analysis of transverse (left) and resliced images (right), revealed only minor differences in those regions which could be directly compared. Clearly the inferior wall is suboptimally evaluated in the transverse images. In the polar representation of pooled data obtained from analysis of resliced images, the outer segments correspond to five basal planes, the inner segments to five mid-ventricular planes, and the innermost segment to the two apical planes.



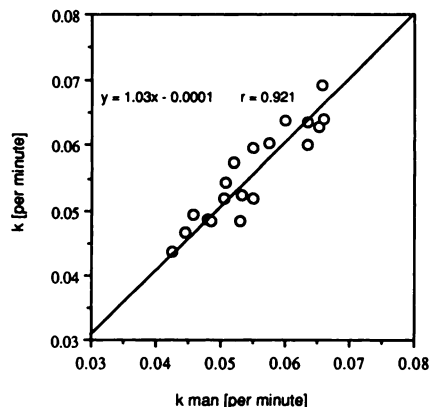


**FIGURE 4**

The global  $^{11}\text{C}$  clearance rate constant ( $k$ ) data obtained from analysis of individual transverse images ( $k_{\text{man}}$ ) were strongly correlated and concordant with the results obtained using the newly developed analysis algorithm for resliced short-axis images.

man heart, monoexponential fitting is less sensitive to statistical noise, more reproducible, and has acceptable overall accuracy (4). A compartmental model of  $^{11}\text{C}$ -acetate tissue kinetics may provide an improvement on the currently used exponential curve fitting approach (25,26).

#### Regional Variation in Physiologic Parameters

It is well recognized that there is, even in the normal heart, regional spatial and temporal heterogeneity in myocardial blood flow and contractile function. However, this variability is generally small, being in the order of 10%–15% (15–17), and its detection *in vivo* has been limited by the spatial and temporal resolution of routinely available imaging modalities. Recent advances in imaging modalities capable of three-dimensional data collection with high spatial and temporal resolution, including ultrafast computed tomography (18–19), rapid cine magnetic resonance imaging (20), and gated cardiac PET (21), have provided evidence of variability of regional left ventricular function in the normal heart.

#### Carbon-11-Acetate Myocardial Uptake

Animal experiments have shown, that  $^{11}\text{C}$ -acetate is avidly extracted by myocardium with an extraction fraction of more than 50% (12). Therefore, initial uptake of this tracer predominantly reflects tracer delivery or blood flow (22,23). Since the  $^{11}\text{C}$ -acetate extraction fraction is <100% and may be sensitive to metabolic alterations, application of this tracer as a quantitative perfusion marker in cardiac disease may be limited. Further studies are required to validate this approach in various disease states, particularly under ischemic conditions. In this study, myocardial  $^{11}\text{C}$ -acetate uptake was homogeneous with a variation of  $12\% \pm 2\%$  in individual studies. Comparison of paired data for  $^{11}\text{C}$ -acetate uptake in the anterior, septal, lateral, and inferior segments revealed no significant regional differences. The lower uptake observed in the apex compared with the mid-ventricular and basal regions reflects under-sampling of the apex due to out-of-plane movement of this segment during systole. This problem may be minimized in the future using ECG-gated data acquisition (21).

#### Carbon-11-Acetate Clearance

The average global  $^{11}\text{C}$  clearance rate constant in our population agrees well with average  $^{11}\text{C}$  clearance rate constants obtained in previous studies (4,10,15). Thus, the average  $^{11}\text{C}$  clearance rate constant in normal subjects at rest appears to be a highly reproducible parameter despite institutional variation of analysis algorithms.

The data demonstrated a small overall variation of regional  $^{11}\text{C}$  clearance rate constants within individual studies ( $10.6\% \pm 2.4\%$ ). However, the observed variation appeared to have a segmental basis since comparison of paired clearance rate constant data suggested the presence of significantly higher clearance in the anterior and septal segments than in the lateral segment ( $p < 0.05$ ). Similarly, there was a significant gradient in clearance rate constants from the basal segments of the heart to the more apical segments ( $p < 0.05$ ) (Fig. 4). In contrast to  $^{11}\text{C}$ -acetate uptake,  $^{11}\text{C}$  clearance kinetics,

**TABLE 4**  
Regional  $^{11}\text{C}$ -acetate Washout Under Different Dietary Conditions

Dietary state	Septal	Anterior	Lateral	Inferior	Apex	Mid-ventricular	Basal
Fasted*	0.059	0.059	0.056	0.058	0.053	0.057	0.060
Oral glucose†	0.056	0.055	0.055	0.056	0.051	0.056	0.056
Eu clamp	0.055	0.057	0.054	0.051	0.050	0.054	0.056
Eu clamp + FFA‡	0.063	0.064	0.058	0.058	0.059	0.061	0.062
All studies§	0.058	0.059	0.056	0.056	0.053	0.057	0.059
s.d.	0.009	0.010	0.009	0.009	0.009	0.009	0.009

\*  $p < 0.05$  for apex versus mid-ventricular and basal.

†  $p < 0.05$  for apex versus mid-ventricular and basal.

‡  $p < 0.05$  for apex versus mid-ventricular and basal; septal versus lateral.

§  $p < 0.05$  for apex versus mid-ventricular and basal; mid-ventricular versus basal; septal versus lateral; anterior versus lateral.

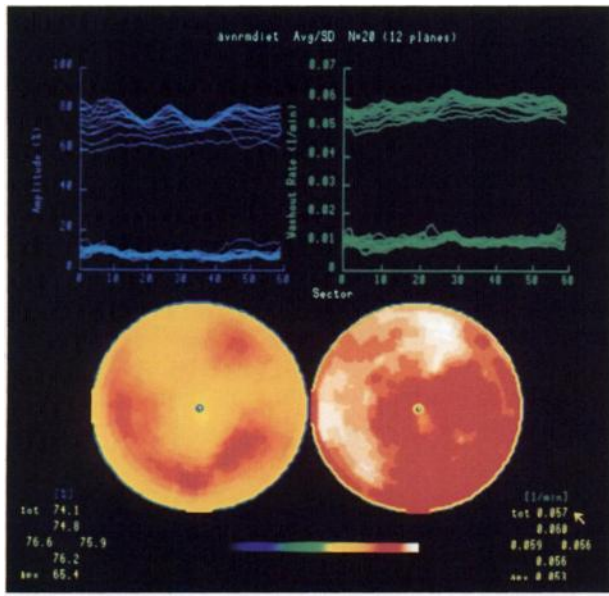


**FIGURE 5**

The upper panel demonstrates circumferential profile data of  $^{11}\text{C}$  uptake (amplitude) and clearance for each of the 12 planes and the standard deviation of these data. Sector 1 corresponds to the posterior intercept of left and right ventricles and is assigned an angle of  $102^\circ$ . Subsequent sectors are orientated counterclockwise and encompass angles of 6 degrees. Polar maps of mean data from the 20 studies (lower panel) reveal relatively homogeneous  $^{11}\text{C}$  uptake (left) but a relative reduction in  $^{11}\text{C}$  clearance in the inferior and lateral segments compared with anterior and septal segments (right).

are insensitive to partial volume and under-sampling of apical activity during systole, reflecting a rate of activity change.

The faster septal  $^{11}\text{C}$  clearance observed in this study is at variance with data reported by Buxton et al. showing slower  $^{11}\text{C}$  clearance in the septum using a closed-chest model in anesthetized dogs (11). However,

Henes et al. (5) also observed faster  $^{11}\text{C}$  clearance in the septum of the normal human heart under resting conditions and following dobutamine infusion. The small but segmental variation may reflect different regional loading conditions or contractile function leading to variation in regional oxygen consumption within the normal human heart. Several studies evaluating myocardial function have described decreasing wall thickening from base to apex of the left ventricle (18,20,21) and are consistent with the observation of decreased  $^{11}\text{C}$  clearance in the apical regions. Further studies directly comparing regional metabolism and contractile function are required to elucidate the mechanism of the suggested regional variation in oxidative metabolism.

#### Effect of Substrate Availability on $^{11}\text{C}$ -acetate Kinetics

Experimental data suggest that myocardial oxygen consumption is dependent on substrate utilization by the heart. In dogs, the utilization of FFAs increased myocardial oxygen consumption significantly when compared with measurements following stimulation of glucose metabolism and inhibition of FFA metabolism (27).

In keeping with these data, comparison of paired studies with and without infusion of fatty acids (Intralipid) in five subjects in this study revealed a small but significant increase of  $^{11}\text{C}$  clearance ( $p < 0.05$ ) in the presence of higher FFA. The effect was most marked in the septal wall. These changes occurred despite a small overall decrease in the average left ventricular double product for these studies, which would be expected to have been associated with a lower average  $^{11}\text{C}$  clearance for this group (Table 1). Although oral glucose load did not change clearance kinetics significantly, there was a slight overall decrease in the average  $^{11}\text{C}$  clearance rate. The faster average  $^{11}\text{C}$  clearance in the fasting state may reflect preferential FFA utilization under these conditions. Armbrecht (4) similarly observed a small decrease in  $^{11}\text{C}$  clearance after oral glucose loading in four subjects.

The interpatient variability in  $^{11}\text{C}$  clearance rate constants was at least two-fold higher in fasting subjects than in subjects following glucose load or under insulin-clamped conditions (Table 1). This possibly reflects the heterogeneity in substrate availability under fasting conditions and suggests that if serial studies or comparison with a normal database is required an attempt should be made to standardize the dietary state of the individuals studied.

#### CONCLUSION

We have described a new method for three-dimensional, quantitative display of  $^{11}\text{C}$ -acetate uptake and

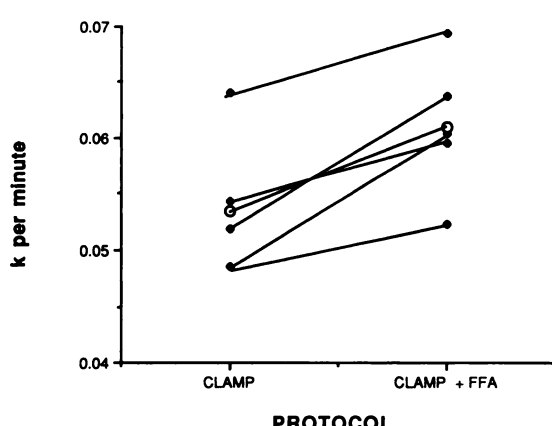


**FIGURE 6**

Global  $^{11}\text{C}$ -acetate clearance rate constants of four patients are shown before and after the addition of FFA infusion to euglycemic hyperinsulinemic clamp (CLAMP). The results demonstrated an increase of  $^{11}\text{C}$  clearance rate constants in all subjects (closed circles), which averaged 15% (open circles).

clearance kinetics which allows objective analysis of myocardial  $^{11}\text{C}$ -acetate uptake and oxidation. This technique has demonstrated relatively homogeneous myocardial uptake and clearance of  $^{11}\text{C}$ -acetate in the normal human heart. There was, however, significant segmental variation in  $^{11}\text{C}$  clearance kinetics, which may represent the effects of regional variation of cardiac work or of substrate utilization. These data suggest that standardization of the metabolic status of subjects undergoing  $^{11}\text{C}$ -acetate studies may be important if this technique is used to describe changes following therapeutic interventions or for comparison with a normal database.

## ACKNOWLEDGMENTS

The authors thank Jill Rothley, CNMT, Leslie Shaw, CNMT, Annette Betley, CNMT, Vincent McCormick, CNMT, for their technical assistance and the cyclotron and radiochemistry staff for preparing  $^{11}\text{C}$ -acetate. Anthony M. Shork, PhD, provided statistical advice.

This work was supported in part by the Clinical Research Council of the University of Michigan and by NIH Grant RO1 HL4107-01 "PET in Myocardial Infarction." This work was completed under the tenure of an established investigatorship from the American Heart Association (M. Schwaiger).

## REFERENCES

- Buxton DB, Schwaiger M, Nguyen A, Phelps ME, Schelbert HR. Radiolabeled acetate as a tracer of myocardial tricarboxylic acid cycle flux. *Circ Res* 1988; 63:628-634.
- Brown MA, Myears DW, Bergmann SR. Validity of estimates of myocardial oxidative metabolism with carbon-11-acetate and positron emission tomography despite altered patterns of substrate utilization. *J Nucl Med* 1989; 30:187-193.
- Schelbert HR, Buxton D. Insights into coronary artery disease gained from metabolic imaging. *Circulation* 1988; 78:496-505.
- Armbrecht JJ, Buxton DB, Brunkun RC, Phelps ME, Schelbert HR. Regional myocardial oxygen consumption determined noninvasively in humans with  $[1-^{11}\text{C}]$ acetate and dynamic positron tomography. *Circulation* 1989; 80:863-872.
- Henes CG, Bergmann SR, Walsh MN, Sobel BE, Geltman EM. Assessment of myocardial oxidative metabolic reserve with positron emission tomography and carbon-11-acetate. *J Nucl Med* 1989; 30:1489-1499.
- DeFronzo RA, Tobin JD, Andres R. Glucose clamp technique: a method for quantifying insulin secretion and resistance. *Am J Physiol* 1979; 237:E214-E223.
- Pike VW, Eakins MN, Allan RM, Selwyn AP. Preparation of  $[1-^{11}\text{C}]$ acetate—an agent for the study of myocardial metabolism by positron emission tomography. *Int J Appl Radiat Isot* 1982; 33:505-512.
- Garcia EV, Van Train K, Maddahi J, et al. Quantification of rotational thallium-201 myocardial tomography. *J Nucl Med* 1985; 26:17-26.
- Hicks K, Ganti G, Mullani N, Gould KI. Automated quantitation of three-dimensional cardiac positron emission tomography for routine clinical use. *J Nucl Med* 1989; 30:1787-1797.
- Walsh MN, Geltman EM, Brown MA, et al. Noninvasive estimation of regional myocardial oxygen consumption by positron emission tomography with carbon-11-acetate in patients with myocardial infarction. *J Nucl Med* 1989; 30:1798-1808.
- Buxton DB, Nienaber CA, Luxen A, et al. Noninvasive quantitation of regional myocardial oxygen consumption in vivo with  $[1-^{11}\text{C}]$ acetate and dynamic positron emission tomography. *Circulation* 1989; 79:134-142.
- Brown M, Marshall DR, Sobel BE, Bergmann SR. Delineation of myocardial oxygen utilization with carbon-11-labeled acetate. *Circulation* 1987; 76:687-696.
- Brown MA, Myears DW, Bergmann SR. Noninvasive assessment of canine myocardial oxidative metabolism with carbon-11-acetate and positron emission tomography. *J Am Coll Cardiol* 1988; 12:1054-1063.
- Graf G, Clausen M, Henze F, Adam WE, Heidenreich P. Schnellverfahren (Flash-SPECT) zur Gewinnung dreidimensionaler Scans der Fourieramplitude und—phase des Herzens mittels der getriggerten single photon emissions computer tomographie (GASPECT). *Nucl Compact* 1989; 20:23-27.
- Bassingthwaite JB, King RB, Roger SA. Fractal nature of regional myocardial blood flow heterogeneity. *Circ Res* 1989; 65:578-590.
- King RB, Bassingthwaite JB. Temporal fluctuations in regional myocardial flows. *Pflügers Arch* 1989; 413:336-342.
- Wolpers HG, Geppert V, Hoeft A, Korb H, Schräder R, Hellige G. Estimation of myocardial blood flow heterogeneity by transorgan helium transport functions. *Pflügers Arch* 1984; 401:217-222.
- Feiring AJ, Rumberger JA, Reiter SJ, et al. Sectional and segmental variability of left ventricular function: experimental and clinical studies using ultrafast computed tomography. *J Am Coll Cardiol* 1988; 12:415-425.
- Rumberger JA, Feiring AJ, Lipton MJ, Higgins CB, Ell SR, Marcus ML. Use of ultrafast computed tomography to quantitate regional myocardial perfusion: a preliminary report. *J Am Coll Cardiol* 1987; 9:59-69.
- Pflugfelder PW, Sechtem UP, White RD, Higgins CB. Quantification of regional myocardial function by rapid cine MR imaging. *AJR* 1988; 150:523-529.
- Yamashita K, Tamaki N, Yonekura Y, et al. Quantitative analysis of regional wall motion by gated myocardial positron emission tomography: validation and comparison. *J Nucl Med* 1989; 30:1775-1786.
- Huang SC, Williams BA, Krivokapich J, Araujo L, Phelps ME, Schelbert HR. Rabbit myocardial  $^{82}\text{Rb}$  kinetics and a compartmental model for blood flow estimation. *Am J Physiol* 1989; 256:H1156-1164.
- Gropler RJ, Henes CG, Moerlein SM, Mintun MA, Siegel BA, Geltman EM. Positron tomographic assessment of relative myocardial perfusion with  $^{11}\text{C}$ -acetate [Abstract]. *Circulation* 1989; 80:II-515.
- Stahl LD, Weiss HR, Becker LC. Myocardial oxygen consumption, oxygen supply/demand heterogeneity, and microvascular patency in regionally stunned myocardium. *Circulation* 1988; 77:865-872.
- Weinberg IN, Huang SC, Hoffman EJ, et al. Validation of PET-acquired input functions for cardiac studies. *J Nucl Med* 1988; 29:241-247.
- Buck A, Hutchins G, Westera G, Schwaiger M. Compartmental model for delineation of myocardial C-11-acetate kinetics [Abstract]. *J Nucl Med* 1990; 31(suppl):777.
- Kahles H, Hellige G, Hunneman DH, Mezger VA, Bretschneider HJ. Influence of myocardial substrate utilization on the oxygen consumption of the heart. *Clin Cardiol* 1982; 5:286-293.